NANOSYSTEMS:
PHYSICS, CHEMISTRY, MATHEMATICS

Kozlova T.O., et al. *Nanosystems: Phys. Chem. Math.*, 2026, **17** (2), 228–235.
http://nanojournal.ifmo.ru
DOI 10.17586/2220-8054-2026-17-2-228-235

Original article

Redox behaviour of nanoscale $ACe_2(PO_4)_3$ (A = NH_4^+, K^+, Rb^+) double ceric phosphates

Taisiya O. Kozlova[1,a], Madina M. Sozarukova[1,b], Daniil A. Kozlov[1,c], Ekaterina D. Sheichenko[1,2,d], Anzhelika O. Bedarkova[1,e], Darya N. Vasilyeva[1,2,f], Alexander E. Baranchikov[1,g], Vladimir K. Ivanov[1,h]

[1]Kurnakov Institute of General and Inorganic Chemistry of the Russian Academy of Sciences, Leninsky prospect, 31, Moscow, 119991, Russia

[2]HSE University, Moscow, Myasnitskaya str., 20, 101000, Russia

[a]taisiya@igic.ras.ru, [b]s_madinam@bk.ru, [c]kozlov@igic.ras.ru, [d]edsheychenko@edu.hse.ru, [e]a.bedarkova@igic.ras.ru, [f]dnvasileva_1@edu.hse.ru, [g]a.baranchikov@yandex.ru, [h]van@igic.ras.ru

Corresponding author: T. O. Kozlova, taisiya@igic.ras.ru

PACS 61.66.Fn; 68.65.-k; 81.70.-q; 82.39.-k

ABSTRACT A comparative study of the redox behaviour of nanocrystalline isostructural $ACe_2(PO_4)_3$ (A = NH_4^+, K^+, Rb^+) double ceric phosphates was performed. It has been established that with respect to alkylperoxyl radicals or hydrogen peroxide as reactive oxygen species, all the double ceric phosphates acted as antioxidants or prooxidants, respectively. The antioxidant activity towards alkylperoxyl radicals was found to be the higher for the phosphates containing potassium or rubidium. Notably, for $KCe_2(PO_4)_3$ and $RbCe_2(PO_4)_3$ an inverse dependence of catalytic activity on concentration in the reaction with H_2O_2 was found, in contrast to $NH_4Ce_2(PO_4)_3$. The redox behaviour of nanoscale cerium dioxide used for comparison was similar to that of ammonium ceric phosphate, but significantly lower in absolute values. This was explained by the suppressive effect of phosphate anions presented in the buffer solutions.

KEYWORDS radical-scavenging ability; prooxidant activity; chemiluminescence; isostructurality.

ACKNOWLEDGEMENTS This work was supported by Russian Science Foundation (Grant no. 23-73-10088, https://rscf.ru/en/project/23-73-10088/) using the equipment of the JRC PMR IGIC RAS.

FOR CITATION Kozlova T.O., Sozarukova M.M., Kozlov D.A., Sheichenko E.D., Bedarkova A.O., Vasilyeva D.N., Baranchikov A.E., Ivanov V.K. Redox behaviour of nanoscale $ACe_2(PO_4)_3$ (A = NH_4^+, K^+, Rb^+) double ceric phosphates. *Nanosystems: Phys. Chem. Math.*, 2026, **17** (2), 228–235.

1. Introduction

Inorganic phosphates comprise both natural and synthetic compounds. They exist in the form of minerals [1], constitute the basis of mammalian bone tissue [2], and are utilized as luminophores [3], ceramics [4, 5], ionic conductors [6], etc. Nowadays, over 200 structural types of inorganic phosphates are known [7]. This crystallochemical diversity arises from a large number of cations that can bind with phosphate tetrahedra in different ways, as well as the ability to substitute or incorporate other anions and molecules (such as H_2O) into the structure [8].

Several studies have been devoted to investigating the influence of cation composition on the functional properties of isostructural compounds [9–13], including inorganic phosphates. In particular, Gautier et al. [14] demonstrated an increase in the second harmonic generation response values for compounds with the composition $A(VO_2)_2(PO_4)\cdot 3H_2O$ (where A = Rb^+, NH_4^+ and K^+). Zhen et al. [15] found the different thermal expansion behavior of isostructural $AZr_2(PO_4)_3$, A = Na^+, K^+, Rb^+, Cs^+. In a similar series, Sukhanov et al. [16] observed a decrease in catalytic activity for methanol dehydration in the order $NaZr_2(PO_4)_3$ > $KZr_2(PO_4)_3$ > $CsZr_2(PO_4)_3$ ≫ $RbZr_2(PO_4)_3$. Patkare et al. [17] evaluated the adsorption capacity for uranyl ions from aqueous solutions for a series of isostructural double thorium phosphates, finding the following trend: $RbTh_2(PO_4)_3$ < $CsTh_2(PO_4)_3$ < $KTh_2(PO_4)_3$.

Despite the extensive knowledge of compounds with the general formula $AM_2^{IV}(PO_4)_3$ (where A = Li–Cs and M = Ti, Zr, Hf or Th, U, Np, Pu), it has not been possible until recently to establish similar composition–structure–property relationships for the M = Ce^{IV} series. This limitation existed due to a lack of information on even one complete structural series of double ceric phosphates. Only in 2025 were the data on the synthesis of $RbCe_2(PO_4)_3$ [18] reported; this compound turned out to be isostructural with two previously known analogues, $NH_4Ce_2(PO_4)_3$ [19] and $KCe_2(PO_4)_3$ [20].

It is known that ceric compounds, primarily nanocrystalline CeO_2, can act as efficient inorganic nanozymes [21–23]. At the same time, cerium(IV) phosphates, owing to their biocompatibility and expected stability in biological environments [24], are equally important to investigate with regard to their biological behavior. So, this study presents the first comparative analysis of the radical-scavenging ability and redox activity of nanoscale isostructural ceric phosphates with the composition $ACe_2(PO_4)_3$ ($A = NH_4^+$, K^+, Rb^+).

2. Experimental Section

The following materials were used as received, without further purification: $Ce(NO_3)_2{\cdot}6H_2O$ (pure grade, Lanhit Russia), potassium hydroxide (pure grade, Sigma Aldrich), rubidium hydroxide (pure grade, Novosibirsk Rare Metals Plant, Russia), aqueous ammonia (25 wt.%, extra-pure grade, Khimmed Russia), phosphoric acid (85 wt.% aq, extra-pure grade, Komponent-Reaktiv, Russia), isopropanol (extra-pure grade, Khimmed Russia), 2,2′-azobis(2-amidinopropane) dihydrochloride (Sigma, #440914), luminol (Sigma, #123072), hydrogen peroxide (extra-pure grade, Khimmed Russia), distilled water.

Previously, using $NH_4Ce_2(PO_4)_3$ and $KCe_2(PO_4)_3$ [25], we developed a synthetic approach to obtain these compounds in a nanoscale state. In the present study, we have accordingly adapted this method to synthesize $RbCe_2^{IV}(PO_4)_3$. First, nanocrystalline (4–5 nm) cerium dioxide (0.100 g) obtained by precipitation from $Ce(NO_3)_3$ aqueous solution was dissolved in concentrated phosphoric acid (5 ml) at 80°C. The cooled solution was placed into an ultrasonic bath Bandelin Sonorex Longlife RK 1050 for 30 min, and then mixed with 35 ml of 1 M KOH, NH_4OH or RbOH aqueous solutions. The obtained gels (∼40 mL) were sonicated using Bandelin Sonopuls HD 3200 homogenizer equipped with titanium horn (TT-13 titanium tip) operated at 20 kHz (amplitude 20%) for 1 h. The resulting suspensions were placed in 100 ml Teflon autoclaves and treated under hydrothermal-microwave (HTMW) conditions at 180°C for 1 h. After cooling the autoclaves, the precipitates were repeatedly washed using distilled water and dried at 60°C in air.

Powder X-ray diffraction (PXRD) patterns were acquired with a DX-2700BH (Haoyuan, China) diffractometer, using Cu $K_{\alpha 1,2}$ radiation in the 2θ range of 5°–80° with 0.02° 2θ steps and a counting time of no less than 1 s per step. The full-profile analysis of diffraction patterns was performed using the Rietveld method realized in the MAUD software (version 2.99) [26]. The diffraction peak profiles were fitted using a pseudo-Voigt function. The sizes of coherent scattering domains (crystallite sizes) and particle anisotropy were estimated using the Lorentzian component of peak broadening and the approach proposed by Popa [27]. For all samples, the crystallite sizes along the (001) direction and in the perpendicular direction were calculated.

Scanning electron microscopy (SEM) images were obtained using an Amber GMH (Tescan, Czech Republic) microscope operated at an accelerating voltage of 5 kV using a secondary electron (Everhart–Thornley) detector. Energy-dispersive X-ray spectroscopy (EDX) was performed using an Ultim Max 100 (Oxford Instruments, UK) detector at an accelerating voltage of 20 kV. Particle size was determined from SEM data using Gwyddion software. To account for anisotropy, the dimensions of each particle were measured in two perpendicular directions. The particle sizes were fitted by a lognormal distribution function.

Analysis of double ceric phosphates redox behaviour in relation to alkylperoxyl radicals or hydrogen peroxide was conducted by chemiluminescent method [28]. Nanocrystalline cerium dioxide powder which was used for the synthesis of double ceric phosphates (see above) was analysed as a control. Directly before the measurements, suspensions of the materials under study were prepared with a concentration of 0.01 M. For this purpose, the powders were dispersed in 5 ml of deionized water and sonicated for 10 min.

Alkylperoxyl radicals were generated by the thermal decomposition of 2,2′-azobis(2-amidinopropane) dihydrochloride (AAPH). For this, 2.5 μM AAPH and 2.0 μM luminol were added to a cuvette containing 100 mM phosphate buffer solution (pH 7.4, 37°C). In experiments with H_2O_2, a reaction mixture of phosphate buffer (100 mM, pH 7.4), hydrogen peroxide (10 mM) and luminol (50 μM) was used. The baseline chemiluminescence signal was monitored for 60–90 s. Upon stabilization of the chemiluminescent signal, the aliquot of ceric phosphate or ceria aqueous dispersion was added.

Detection of the chemiluminescence signal was carried out using a DISoft (Russia) Lum-1200 instrument equipped with 12 detection channels. The experiments were performed with three replicates for each sample. The results were processed using PowerGraph software (version 3.3).

3. Results and discussion

The isostructural nature of the compounds obtained was confirmed by X-ray phase analysis (Fig. 1). The calculated unit cell parameters for the synthesised double ceric phosphates are given in Table 1 and agree well with previously reported data [18–20]. From the data presented in Table 1 it follows that an increase in the cation size ($K^+ < NH_4^+ < Rb^+$ [14, 29, 30]) results in the expansion of the volumes of the corresponding unit cells due to the increase in the a and b parameter values. The crystallite sizes calculated in two crystallographic directions were found to be less than 100 nm (Table 1), with the smallest value for the $RbCe_2(PO_4)_3$ phase, and the largest for the $NH_4Ce_2(PO_4)_3$ phase. Scanning electron microscopy images confirm particle anisotropy, and the particle sizes were found to be close to the XRD data (Fig. 2). The chemical composition was confirmed by EDX analysis.

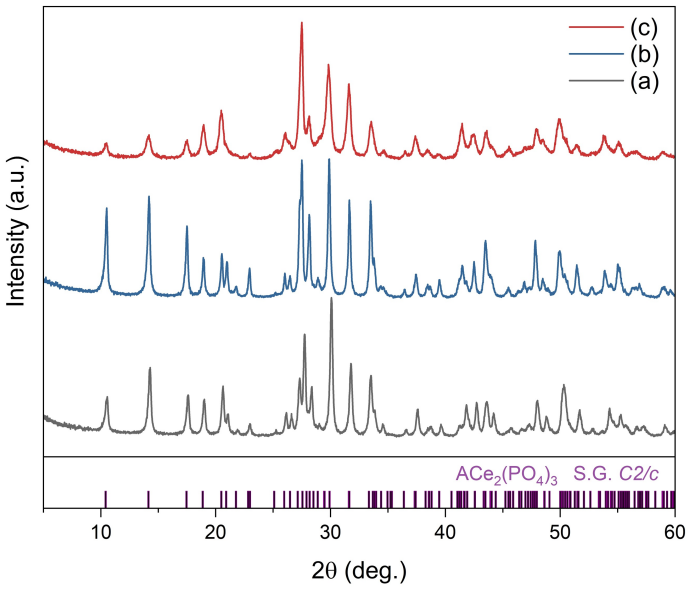

FIG. 1. Powder X-ray diffraction patterns of the products of HTMW treatment of ceric phosphate gels formed upon the addition of 1 M KOH (a), NH_4OH (b) or RbOH (c) aqueous solutions to ceric phosphate solutions. The corresponding Bragg peak positions for $ACe_2(PO_4)_3$ (A = NH_4^+, K^+, Rb^+) are shown below

TABLE 1. Structural parameters and crystallite sizes for the products of HTMW treatment of ceric phosphate gels formed upon the addition of 1 M KOH, NH_4OH or RbOH to ceric phosphate solutions

Sample	KCeP	NCeP	RbCeP
Precipitating agent	1 M KOH aqueous solution	1 M NH_4OH aqueous solution	1 M RbOH aqueous solution
Phase composition	$KCe_2(PO_4)_3$	$NH_4Ce_2(PO_4)_3$	$RbCe_2(PO_4)_3$
Lattice parameters	S.G. *C2/c* $a = 17.3764(8)$ Å $b = 6.7316(3)$ Å $c = 7.9700(4)$ Å $\beta = 102.292(3)^\circ$	S.G. *C2/c* $a = 17.4749(7)$ Å $b = 6.7711(3)$ Å $c = 7.9988(3)$ Å $\beta = 102.794(3)^\circ$	S.G. *C2/c* $a = 17.502(1)$ Å $b = 6.7804(6)$ Å $c = 7.9867(7)$ Å $\beta = 102.847(5)^\circ$
Crystallite size, nm	$\langle D\rangle_{001} = 60 \pm 3$ $\langle D\rangle_{110} = 70 \pm 3$	$\langle D\rangle_{001} = 110 \pm 5$ $\langle D\rangle_{110} = 78 \pm 2$	$\langle D\rangle_{001} = 28 \pm 2$ $\langle D\rangle_{110} = 36 \pm 3$

The redox behaviour of the synthesized isostructural compounds was evaluated in model systems. Experiments were based on monitoring the chemiluminescence intensity from the oxidation of luminol by alkylperoxyl radicals (ROO•) or hydrogen peroxide decomposition products.

In the first assay, introducing the samples into a reaction solution resulted in a decrease in luminol-dependent chemiluminescence compared to the control (Fig. 3). The degree of chemiluminescence inhibition varied among the samples, reflecting their different radical-scavenging capacities (Fig. 3a). Overall, the observed kinetic profiles are characteristic of long-acting antioxidants that scavenge free radicals at a relatively low rate [31].

To quantitatively evaluate the radical-scavenging properties of the nanoscale $NH_4Ce_2(PO_4)_3$, $KCe_2(PO_4)_3$ and $RbCe_2(PO_4)_3$ samples, the areas of the luminescence suppression region (S_{CL}, a.u.) were calculated. This parameter is proportional to the number of the scavenged radicals and reflects the antioxidant capacity of a material (Fig. 3b).The $KCe_2(PO_4)_3$ and $RbCe_2(PO_4)_3$ samples showed the most pronounced antioxidant activity against organic radicals compared to the ammonium-containing analogue. This difference is likely attributable to the smaller particle size of the potassium and rubidium ceric phosphates, which leads to a higher concentration of surface-active sites (e.g., Ce^{3+}/Ce^{4+}

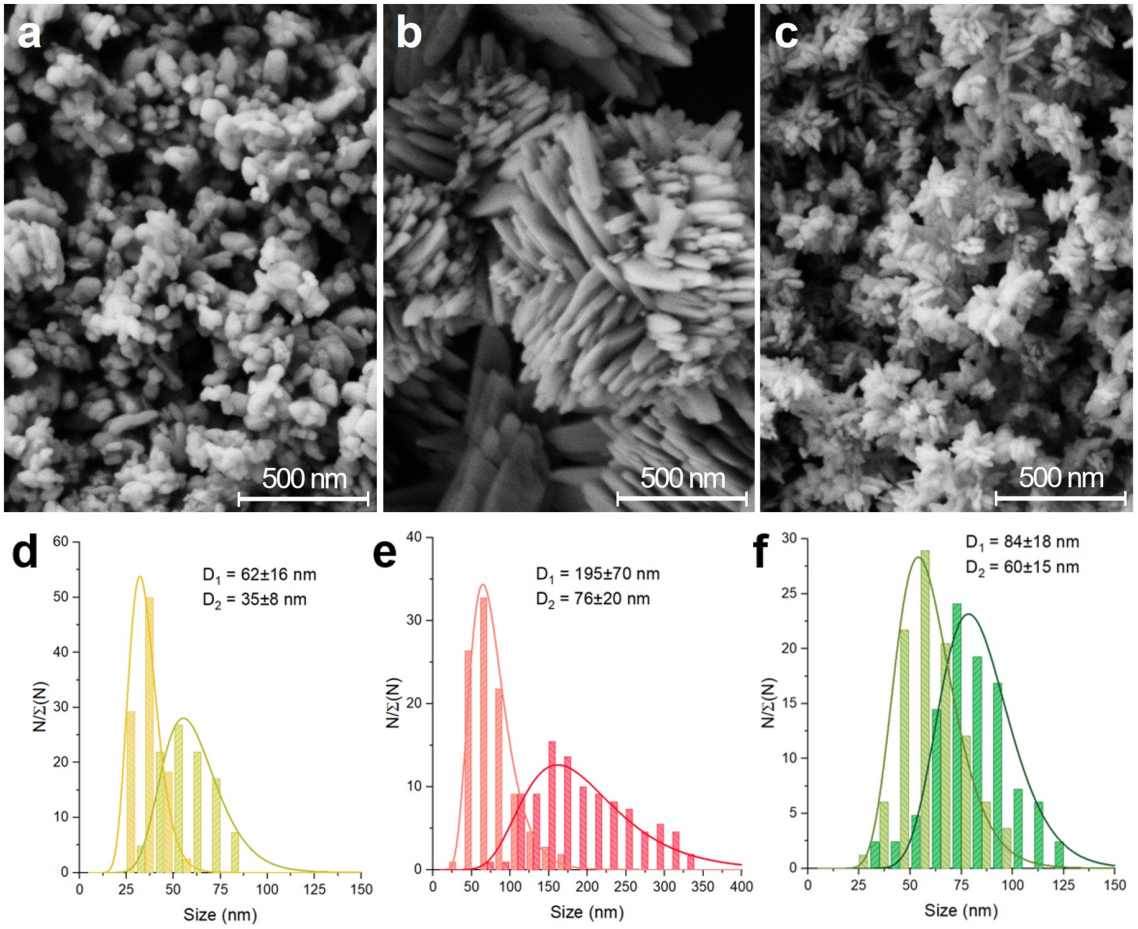

FIG. 2. SEM images and corresponding particle size distribution of KCeP (a,d), NCeP (b,e), RbCeP (c,f)

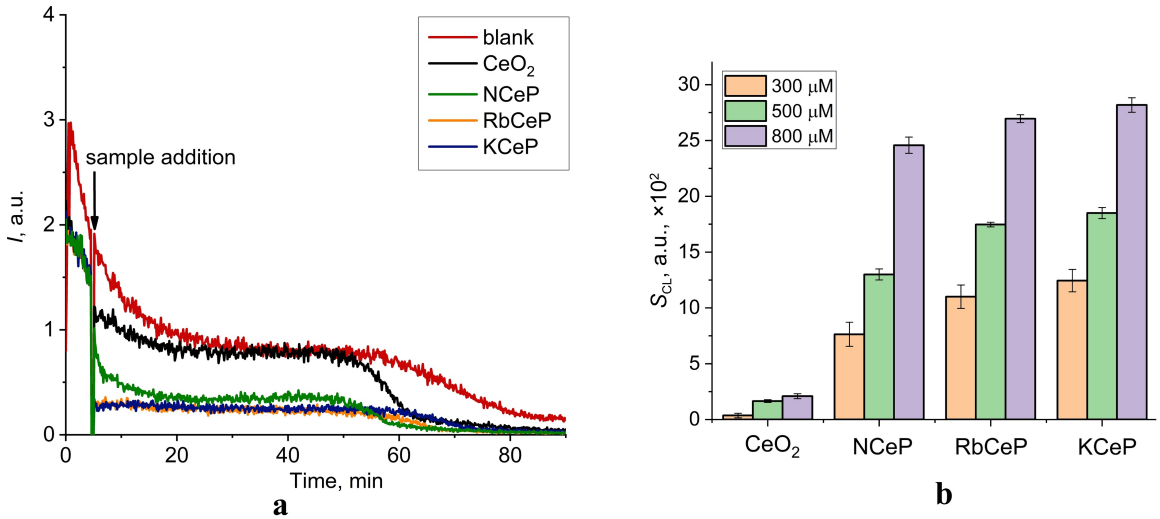

FIG. 3. a) Chemiluminograms characterising the radical-scavenging properties of CeO_2, $NH_4Ce_2(PO_4)_3$, $KCe_2(PO_4)_3$ and $RbCe_2(PO_4)_3$ (800 μM); b) histograms of chemiluminescence suppression (S_{CL}, a.u.) for ceric samples

ratio, oxygen vacancies and hydroxyl groups) [32–35] available for interaction with the components of the studied mixture, including free radicals. Nanocrystalline cerium dioxide (4–5 nm) demonstrated the weakest antioxidant effect, in contrast to the ceric phosphate suspensions. Since chemiluminescence was recorded under physiologically relevant conditions (100 mM PBS, pH 7.4), this result aligns with literature reports on the inhibitory effect of phosphate ions on CeO_2 activity. Inorganic phosphates and phosphate-containing molecules, which are abundant in biological environments, are known to adsorb onto the surface of ceria nanoparticles and significantly suppress their catalytic properties [36–38].

Fig. 4 shows chemiluminograms obtained by adding suspensions of double ceric phosphates or cerium dioxide to a reaction mixture containing H_2O_2 and luminol (pH 7.4, phosphate buffer solution).

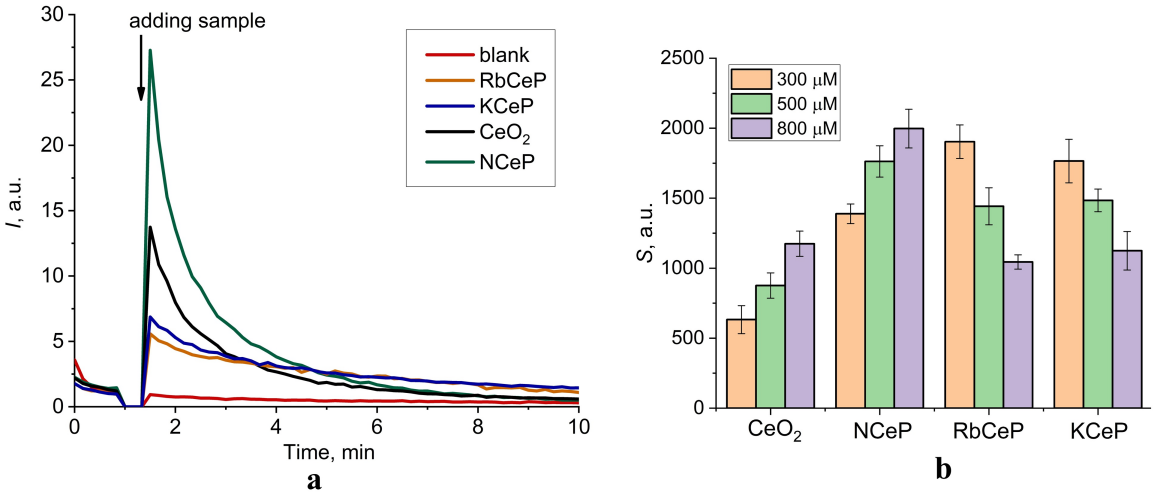

FIG. 4. a) Chemiluminograms characterising prooxidant activity of the of CeO_2, $NH_4Ce_2(PO_4)_3$, $KCe_2(PO_4)_3$ and $RbCe_2(PO_4)_3$ (800 μM); b) light sums (S) as a function of ceric samples concentrations

Upon addition of the studied samples, a sharp, exponentially decaying increase in luminol-dependent chemiluminescence was observed (Fig. 4a). This luminescence burst, caused by the generation of reactive oxygen species (ROS), indicates the prooxidant properties of the compounds, consistent with data reported for other ceria-based nanomaterials [39, 40]. Notably, the samples exhibit two distinct types of chemiluminescence kinetics: CeO_2 and $NH_4Ce_2(PO_4)_3$ show a sharp exponential decay whereas $RbCe_2(PO_4)_3$ and $KCe_2(PO_4)_3$ produce flatter curves. The flatter profiles for the rubidium and potassium ceric phosphates likely result from their lower reaction rate with hydrogen peroxide compared to CeO_2 and $NH_4Ce_2(PO_4)_3$.

For the quantitative assessment of prooxidant properties, we used the integral area under the chemiluminescence curve (S) over a selected 5-minute period. This value is proportional to the amount of ROS generated. The data in Fig. 4b show a dose-dependent increase in chemiluminescence for CeO_2 and $NH_4Ce_2(PO_4)_3$ nanoparticles. In contrast, the $RbCe_2(PO_4)_3$ and $KCe_2(PO_4)_3$ samples exhibited a decrease in prooxidant activity with increasing suspensions concentration. This inverse relationship between prooxidant activity and nanoparticle concentration is unusual. The most probable reasons for this behavior, found in isolated examples from the literature, include the aggregation of nanoparticles, leading to a decrease in the number of available surface-active sites [41], or ROS scavenging at high concentrations of compounds [42–44]. The first explanation is unlikely, as such a reversible concentration-dependent relationship was not observed in experiments with alkylperoxyl radicals. Therefore, we hypothesize that for potassium and rubidium ceric phosphates, an increase in concentration promotes the scavenging of reactive oxygen species, which competes with the decomposition of H_2O_2.

Thus, using two model systems, we have demonstrated for the first time the difference in redox behavior between $NH_4Ce_2(PO_4)_3$ and its isostructural potassium or rubidium analogues. Although the precise reasons for their different redox activities cannot yet be definitively established, they are likely related to the cation type (NH_4^+ or K^+, Rb^+) [45,46]. Several studies have demonstrated differences in the physicochemical properties of isostructural compounds containing ammonium or alkali metal cations. For instance, it was shown that $NH_4Zn_2BO_3Cl_2$ exhibits superior nonlinear optical properties compared to its $KZn_2BO_3Cl_2$ or $RbZn_2BO_3Cl_2$ analogues, attributed to a higher interlayer binding energy [47]. In another study, Johnson [48] calculated the solubility of ammonium perrhenate (H_4ReO_4) to be considerably greater than that of the potassium and rubidium salts (0.274, 0.0410, and 0.037 mol/kg, respectively). It is also necessary to pay attention to the different thermal behavior of $NH_4Ce_2(PO_4)_3$ compared to $KCe_2(PO_4)_3$ and $RbCe_2(PO_4)_3$. Thus, during the thermolysis of $NH_4Ce_2(PO_4)_3$, only $CePO_4$ formation and NO release were observed, presumably due to the oxidation of ammonia by redox active species, such as ceric cations [19]. In contrast, the thermolysis of the potassium and rubidium analogues leads to the crystallization of monazite ($CePO_4$) alongside KPO_3 [20] or $RbPO_3$ [18] polyphosphates, respectively.

The results obtained in this study indicate that nanocrystalline double ceric phosphates $ACe_2(PO_4)_3$ ($A = NH_4^+$, K^+, Rb^+) exhibit dual concentration-dependent antioxidant/prooxidant behaviour. These findings provide a starting point for further in-depth study of ceric phosphates redox activity, which could contribute to developing new approaches for preventing and treating diseases associated with oxidative stress [49, 50].

4. Conclusions

This study represents the first comparative analysis of the redox activity of isostructural double ceric phosphates, containing a monovalent cation. Compounds with the general composition $ACe_2^{IV}(PO_4)_3$ ($A = NH_4^+$, K^+, Rb^+) and particle sizes less than 100 nm were successfully synthesized under hydrothermal-microwave treatment. Chemiluminescence analysis using two model test systems demonstrated that the nature of the second cation in the studied ceric phosphates significantly influences their redox properties. Specifically, suppression of chemiluminescence induced by alkylperoxyl radicals was found to be more pronounced for potassium and rubidium ceric phosphates than for their ammonium counterpart. A qualitative difference in the behavior of the studied compounds was observed in the chemiluminescent reaction of H_2O_2 catalytic decomposition. Thus, $NH_4Ce_2(PO_4)_3$ demonstrated an increase in prooxidant activity with concentration growth, while $KCe_2(PO_4)_3$ and $RbCe_2(PO_4)_3$ showed an unusual inverse dose-response relationship. These results highlight the important role of the cation composition in modulating the biochemical properties of cerium-containing nanomaterials, expanding the potential for their use as controlled pro-/antioxidant agents.

References

[1] Achary S.N., Bevara S., Tyagi A.K. Recent Progress on Synthesis and Structural Aspects of Rare-Earth Phosphates. *Coord. Chem. Rev.*, 2017, **340**, P. 266–297.

[2] Lukaviciute L., Ganceviciene R., Tsuru K., Ishikawa K., Yang J.-C., Grigoraviciute I., Kareiva A. Cationic Substitution Effects in Phosphate-Based Bioceramics – A Way towards Superior Bioproperties. *Ceram. Int.*, 2024, **50**, P. 34479–34509.

[3] Peter A.M., Kailasnath M. Perspectives of Low Dimensional Luminescent Rare Earth Phosphates: Applications and Challenges. In *Low-Dimensional Materials, Systems and Applications*, Volume 1, Elsevier, 2026, P. 443–478.

[4] Clavier N., Podor R., Dacheux N. Crystal Chemistry of the Monazite Structure. *J. Eur. Ceram. Soc.*, 2011, **31**, P. 941–976.

[5] Neumeier S., Arinicheva Y., Ji Y., Heuser J.M., Kowalski P.M., Kegler P., Schlenz H., Bosbach Di. Deissmann G. New Insights into Phosphate Based Materials for the Immobilisation of Actinides. *Radiochim. Acta*, 2017, **105**, P. 961–984.

[6] Chiang S.-J., Kaduk J.A., Shaw L.L. High Ionic Conducting NaSICON Enabled by Mechanical Activation Enhanced Reaction. *Mater. Chem. Phys.*, 2024, **312**, P. 128656.

[7] Ameen S., Shaheer Akhtar M. Introductory Chapter: An Overview of Phosphate Mineral and Electrochemical Detection of Phosphate for Environmental Remediation. In *Functional Phosphate Materials and Their Applications*, IntechOpen, 2023.

[8] Attfield J.P. Phosphates: Solid-State Chemistry. In *Encyclopedia of Inorganic and Bioinorganic Chemistry*, Wiley, 2004, P. 1–16.

[9] Pet'kov V.I., Shipilov A.S., Sukhanov M. V. Thermal Expansion of $MZr_2(AsO_4)_3$ and $MZr_2(TO_4)_x(PO_4)_{3-x}$ (M = Li, Na, K, Rb, Cs; T = As, V). *Inorg. Mater.*, 2015, **51**, P. 1079–1085.

[10] Huang H., Kong X., Zhao H., Ye N., Hu Z., Li C. A-Site Cation Substitution toward Structural Transformation in Phosphates Exhibiting Short UV Transparency and Second Harmonic Response. *Inorg. Chem.*, 2025, **64**, P. 17083–17090.

[11] Ermilova M.M., Sukhanov M.V., Borisov R.S., Orekhova N.V., Pet'kov V.I. Novikova S.A., Il'in A.B., Yaroslavtsev A.B. Synthesis of the New Framework Phosphates and Their Catalytic Activity in Ethanol Conversion into Hydrocarbons. *Catal. Today*, 2012, **193**, P. 37–41.

[12] Slobodin V., Surat L.L., Zubkov V.G., Tyutyunnik A.P., Berger I.F., Kuznetsov M.V., Perelyaeva L.A., Shein I.R., Ivanovskii A.L., Shulgin B.V., Solomonov V. I., Svensson G., Forslund B., Sayagués M. J. Structural, Luminescence, and Electronic Properties of the Alkaline Metal-Strontium Cyclotetravanadates $M_2Sr(VO_3)_4$, (M=Na, K, Rb, Cs). *Phys. Rev. B*, 2005, **72**, P. 155205.

[13] Wen M., Wu H., Wu X. Influence of Cation on the Anion Frameworks and Properties of Four Lead Phosphates, $A_2PbBi_2(PO_4)_2(P_2O_7)$ (A = Rb, Cs) and $A_2PbP_2O_7$ (A = K, Rb). *Inorg. Chem.*, 2020, **59**, P. 2945–2951.

[14] Gautier R., Auguste S., Clevers S., Dupray V., Coquerel G., Le Fur E. Influence of the Cation Size on the Second Harmonic Generation Response of Chiral $A(VO_2)_2(PO_4)\cdot 3H_2O$ ($A = K^+$, NH_4^+ and Rb^+). *CrystEngComm*, 2014, **16**, P. 10902–10906.

[15] Zhen X., Sanson A., Sun Q., Liang E., Gao Q. Role of Alkali Ions in the Near-Zero Thermal Expansion of NaSICON-Type $AZr_2(PO_4)_3$ (A=Na, K, Rb, Cs) and $Zr_2(PO_4)_3$ Compounds. *Phys. Rev. B*, 2023, **108**, P. 144102.

[16] Sukhanov M.V., Ermilova M.M., Orekhova N.V., Pet'kov V.I., Tereshchenko G.F. Catalytic Properties of Zirconium Phosphate and Double Phosphates of Zirconium and Alkali Metals with a $NaZr_2(PO_4)_3$ Structure. *Russ. J. Appl. Chem.*, 2006, **79**, P. 614–618.

[17] Patkare G., Shafeeq M., Sengupta A., Keskar M., Phatak R., Kannan S. Investigation of the Thermal Properties of Alkali Metal Thorium Phosphates and Their Application for the Sorption of Uranyl Ion from Acidic Medium. *Eur. J. Inorg. Chem.*, 2023, **26**, P. 202300140.

[18] Vasilyeva D.N., Kozlov D.A., Protsenko M.R., Simonenko N.P., Kozlova T.O. Ivanov V.K. Structure and Thermal Behavior of Novel Double Ceric Phosphates $RbCe_2(PO_4)_3$and $Rb_2Ce(PO_4)_2 \cdot xH_2O$. *Russ. J. Inorg. Chem.*, 2025, **70**, P. 943–951.

[19] Shekunova T.O., Istomin S.Y., Mironov A. V., Baranchikov A.E., Yapryntsev A.D., Galstyan A.A., Simonenko N.P., Gippius A.A., Zhurenko S.V., Shatalova T.B., et al. Crystallization Pathways of Cerium(IV) Phosphates Under Hydrothermal Conditions: A Search for New Phases with a Tunnel Structure. *Eur. J. Inorg. Chem.*, 2019, **2019**, P. 3242–3248.

[20] Kozlova T.O., Vasilyeva D.N., Kozlov D.A., Teplonogova M.A., Baranchikov A.E., Simonenko N.P., Ivanov V.K. Synthesis and Thermal Behavior of $KCe_2(PO_4)_3$, a New Full-Member in the $A^IM^{IV}{}_2(PO_4)_3$ Family. *Nanosyst. Physics, Chem. Math.*, 2023, **14**, P. 112–119.

[21] Pansambal S., Oza R., Borgave S., Chauhan A., Bardapurkar P., Vyas S., Suresh G. Bioengineered Cerium Oxide (CeO_2) Nanoparticles and Their Diverse Applications: A Review. *Appl. Nanosci.*, 2023, **13**, P. 6067–6092.

[22] Nag S., Mitra O. P, S., Bhattacharjee A., Mohanto S., Gowda B.H.J., Kar S., Ramaiah S., Anbarasu A., Ahmed M.G. Exploring the Emerging Trends in the Synthesis and Theranostic Paradigms of Cerium Oxide Nanoparticles (CeONPs): A Comprehensive Review. *Mater. Today Chem.*, 2024, **35**, P. 101894.

[23] Lord M.S., Berret J.F., Singh S., Vinu A., Karakoti A.S. Redox Active Cerium Oxide Nanoparticles: Current Status and Burning Issues. *Small*, 2021, **17**, P. 2102342.

[24] Kozlova T.O., Popov A.L., Kolesnik I. V., Kolmanovich D.D., Baranchikov A.E., Shcherbakov A.B., Ivanov V.K. Amorphous and Crystalline Cerium(IV) Phosphates: Biocompatible ROS-Scavenging Sunscreens. *J. Mater. Chem. B*, 2022, **10**, P. 1775–1785.
[25] Kozlova T.O., Sheichenko E.D., Vasilyeva D.N., Kozlov D.A., Kolesnik I.V., Tronev I.V, Teplonogova M.A., Baranchikov A.E., Ivanov V.K. Ultrasonic-Assisted Hydrothermal Synthesis of Nanoscale Double Ceric Phosphates. *Nanosyst. Physics, Chem. Math.*, 2024, **15**, P. 215–223.
[26] Lutterotti L. Total pattern fitting for the combined size-strain-stress-texture determination in thin film diffraction. *Nucl. Instrum. Methods Phys. Res. B*, 2010, **268**, P. 334–340.
[27] Popa, N.C. The (hkl) Dependence of Diffraction-Line Broadening Caused by Strain and Size for all Laue Groups in Rietveld Refinement. *J. Appl. Crystallogr*, 1998, **31**, P. 176–180.
[28] Alekseev A.V., Proskurnina E.V., Vladimirov Y.A. Determination of Antioxidants by Sensitized Chemiluminescence Using 2,2'-Azo-Bis(2-Amidinopropane). *Moscow Univ. Chem. Bull.*, 2012, **67**, P. 127–132.
[29] Sidey V. On the Effective Ionic Radii for Ammonium. *Acta Crystallogr. Sect. B Struct. Sci. Cryst. Eng. Mater.*, 2016, **72**, P. 626–633.
[30] Shannon R.D., Prewitt C.T. Effective Ionic Radii in Oxides and Fluorides. *Acta Crystallogr. Sect. B Struct. Crystallogr. Cryst. Chem.*, 1969, **25**, P. 925–946.
[31] Vladimirov G.K., Sergunova E. V., Izmaylov D.Y., Vladimirov Y.A. Chemiluminescent Determination of Total Antioxidant Capacity in Medicinal Plant Material. *Bull. Russ. State Med. Univ.*, 2016, P. 62–68.
[32] Lee S.S., Song W., Cho M., Puppala H.L., Nguyen P., Zhu H., Segatori L., Colvin V.L. Antioxidant Properties of Cerium Oxide Nanocrystals as a Function of Nanocrystal Diameter and Surface Coating. *ACS Nano*, 2013, **7**, P. 9693–9703.
[33] Ghosalya M.K., Li X., Beck A., van Bokhoven J.A., Artiglia L. Size of Ceria Particles Influences Surface Hydroxylation and Hydroxyl Stability. *J. Phys. Chem. C.*, 2021, **125**, P. 9303–9309.
[34] Römer I., Briffa S.M., Arroyo Rojas Dasilva Y., Hapiuk D., Trouillet V., Palmer R.E., Valsami-Jones E. Impact of Particle Size, Oxidation State and Capping Agent of Different Cerium Dioxide Nanoparticles on the Phosphate-Induced Transformations at Different PH and Concentration. *PLoS One*, 2019, **14**, P. e0217483.
[35] Listova A.L., Kuzenkova A.S., Gerasimov M.A., Kulikova E.S., Svetogorov R.D., Novichkov D.A., Averin A.A., Yapaskurt V.O., Romanchuk A.Y., Kalmykov S.N., Plakhova T.V. Comprehensive Dissolution Study on Two Double Ce(IV) Phosphates with Evidence of Secondary CeO_2 Nanoparticle Formation. *Molecules*, 2025, **30**, P. 2105.
[36] Ta K.M., Neal C.J. Coathup M.J., Seal S., Phillips R.M., Molinari M. The Interaction of Phosphate Species with Cerium Oxide: The Known, the Ambiguous and the Unexplained. *Biomater. Adv.*, 2025, **166**, P. 214063.
[37] Singh S., Dosani T., Karakoti A.S., Kumar A., Seal S., Self W.T. A Phosphate-Dependent Shift in Redox State of Cerium Oxide Nanoparticles and Its Effects on Catalytic Properties. *Biomaterials*, 2011, **32**, P. 6745–6753.
[38] Singh R., Singh S. Role of Phosphate on Stability and Catalase Mimetic Activity of Cerium Oxide Nanoparticles. *Colloids Surfaces B Biointerfaces*, 2015, **132**, P. 78–84.
[39] Sozarukova M.M., Proskurnina E.V, Ivanov V.K. Prooxidant Potential of CeO_2 Nanoparticles towards Hydrogen Peroxide. *Nanosyst. Physics, Chem. Math.*, 2021, **12**, P. 283–290.
[40] Sozarukova M.M., Kozlova T.O., Beshkareva T.S., Popov A.L., Kolmanovich D.D., Vinnik D.A., Ivanova O.S., Lukashin A. V., Baranchikov A.E., Ivanov V.K. Gadolinium Doping Modulates the Enzyme-like Activity and Radical-Scavenging Properties of CeO_2 Nanoparticles. *Nanomaterials*, 2024, **14**, 769.
[41] Xu C., Qu X. Cerium Oxide Nanoparticle: A Remarkably Versatile Rare Earth Nanomaterial for Biological Applications. *NPG Asia Mater.*, 2014, **6**, P. e90.
[42] Joubert El., Winterton P., Britz T.J., Gelderblom W.C.A. Antioxidant and Pro-Oxidant Activities of Aqueous Extracts and Crude Polyphenolic Fractions of Rooibos (Aspalathus Linearis). *J. Agric. Food Chem.*, 2005, **53**, P. 10260–10267.
[43] Nowak M., Tryniszewski W., Sarniak A., Wlodarczyk A., Nowak P.J., Nowak D. Concentration Dependence of Anti- and Pro-Oxidant Activity of Polyphenols as Evaluated with a Light-Emitting Fe^{2+}-Egta-H_2O_2 System. *Molecules*, 2022, **27**, P. 3453.
[44] Stoeva S., Hvarchanova N., Georgiev K.D., Radeva-Ilieva, M. Green Tea: Antioxidant vs. Pro-Oxidant Activity. *Beverages*, 2025, **11**, P. 64.
[45] Hoard J.L., Blair V. The Crystal Structures of Rubidium and Ammonium Fluoborates. *J. Am. Chem. Soc.*, 1935, **57**, P. 1985–1988.
[46] Aydin F., Zhan C., Ritt C., Epsztein R., Elimelech M., Schwegler E., Pham T.A. Similarities and Differences between Potassium and Ammonium Ions in Liquid Water: A First-Principles Study. *Phys. Chem. Chem. Phys.*, 2020, **22**, P. 2540–2548.
[47] Yang G., Gong P., Lin Z., Ye N. $AZn_2BO_3X_2$ (A = K, Rb, NH_4; X = Cl, Br): New Members of KBBF Family Exhibiting Large SHG Response and the Enhancement of Layer Interaction by Modified Structures. *Chem. Mater.*, 2016, **28**, P. 9122–9131.
[48] Johnson D.A. Thermochemistry of Ammonium and Rubidium Perrhenates, and the Effect of Hydrogen Bonding on the Solubilities of Ammonium Salts. *J. Chem. Soc. Dalt. Trans.*, 1990, P. 3301–3304.
[49] Castañeda-Arriaga R., Pérez-Gonzalez A., Reina M., Alvarez-Idaboy J.R., Galano A. Comprehensive Investigation on the Antioxidant and Pro-Oxidant Effects of Phenolic Compounds: A Double-Edged Sword in the Context of Oxidative Stress? *J. Phys. Chem. B*, 2018, **122**, P. 6198–6214.
[50] Samrot A.V., Singh S.P.R., Deenadhayalan R., Rajesh V.V., Padmanaban S., Radhakrishnan K.K. Nanoparticles, a Double-Edged Sword with Oxidant as Well as Antioxidant Properties – A Review. *Oxygen*, 2022, **2**, P. 591–604.

Submitted 17 February 2026; revised 31 March 2026; accepted 1 April 2026

Information about the authors:

Taisiya O. Kozlova – Kurnakov Institute of General and Inorganic Chemistry of the Russian Academy of Sciences, Leninsky prospect, 31, Moscow, 119991, Russia; ORCID 0000-0002-9757-9148; taisiya@igic.ras.ru

Madina M. Sozarukova – Kurnakov Institute of General and Inorganic Chemistry of the Russian Academy of Sciences, Leninsky prospect, 31, Moscow, 119991, Russia; ORCID 0000-0002-5868-4746; s_madinam@bk.ru

Daniil A. Kozlov – Kurnakov Institute of General and Inorganic Chemistry of the Russian Academy of Sciences, Leninsky prospect, 31, Moscow, 119991, Russia; ORCID 0000-0003-0620-8016; kozlov@igic.ras.ru

Ekaterina D. Sheichenko – Kurnakov Institute of General and Inorganic Chemistry of the Russian Academy of Sciences, Leninsky prospect, 31, Moscow, 119991, Russia; HSE University, Moscow, Myasnitskaya str., 20, 101000, Russia; ORCID 0000-0003-3485-1842; edsheychenko@edu.hse.ru

Anzhelika O. Bedarkova – Kurnakov Institute of General and Inorganic Chemistry of the Russian Academy of Sciences, Leninsky prospect, 31, Moscow, 119991, Russia; ORCID 0000-0003-4346-5644; a.bedarkova@igic.ras.ru

Darya N. Vasilyeva – Kurnakov Institute of General and Inorganic Chemistry of the Russian Academy of Sciences, Leninsky prospect, 31, Moscow, 119991, Russia; HSE University, Moscow, Myasnitskaya str., 20, 101000, Russia; ORCID 0009-0004-3560-4178; dnvasileva_1@edu.hse.ru

Alexander E. Baranchikov – Kurnakov Institute of General and Inorganic Chemistry of the Russian Academy of Sciences, Leninsky prospect, 31, Moscow, 119991, Russia; ORCID 0000-0002-2378-7446; a.baranchikov@yandex.ru

Vladimir K. Ivanov – Kurnakov Institute of General and Inorganic Chemistry of the Russian Academy of Sciences, Leninsky prospect, 31, Moscow, 119991, Russia; ORCID 0000-0003-2343-2140; van@igic.ras.ru

Conflict of interest: the authors declare no conflict of interest.